How to cite: Angew. Chem. Int. Ed. 2023, 62, e202309440
doi.org/10.1002/anie.202309440

Polymerization Hot Paper

Tribochemically Controlled Atom Transfer Radical Polymerization Enabled by Contact Electrification

Chen Wang, Ruoqing Zhao, Wenru Fan, Lei Li, Haoyang Feng, Zexuan Li, Ci Yan, Xiaoyang Shao, Krzysztof Matyjaszewski,* and Zhenhua Wang**

Abstract: Traditional mechanochemically controlled reversible-deactivation radical polymerization (RDRP) utilizes ultrasound or ball milling to regenerate activators, which induce side reactions because of the high-energy and high-frequency stimuli. Here, we propose a facile approach for tribochemically controlled atom transfer radical polymerization (tribo-ATRP) that relies on contact-electro-catalysis (CEC) between titanium oxide (TiO_2) particles and $CuBr_2$/tris(2-pyridylmethylamine (TPMA), without any high-energy input. Under the friction induced by stirring, the TiO_2 particles are electrified, continuously reducing $CuBr_2$/TPMA into CuBr/TPMA, thereby conversing alkyl halides into active radicals to start ATRP. In addition, the effect of friction on the reaction was elucidated by theoretical simulation. The results indicated that increasing the frequency could reduce the energy barrier for the electron transfer from TiO_2 particles to $CuBr_2$/TPMA. In this study, the design of tribo-ATRP was successfully achieved, enabling CEC (ca. 10 Hz) access to a variety of polymers with predetermined molecular weights, low dispersity, and high chain-end fidelity.

Reversible-deactivation radical polymerization (RDRP) has offered intriguing possibilities for the rational design of polymers with desired chain length, tunable dispersity and high chain-end fidelities.[1] Recently, the convergence of RDRP and piezocatalysis has enabled access to a large range of polymers, gels and hybrids, with the ability to modify their macromolecular structure in response to mechanical stimuli.[2] Atom transfer radical polymerization (ATRP)[3] and reversible addition-fragmentation chain-transfer (RAFT)[4] polymerization are the most prevailing RDRP techniques with highly effective feasibility and tolerance to functional groups.[5] The key to achieving mechanochemically controlled ATRP and RAFT is the regeneration of active species by ultrasound[6] or ball milling.[7] A wide range of deactivators, including Cu^{II}, aryldiazonium salts,[8] and thiols,[9] have been converted into radicals or activators for initiating RDRP by the polarized piezoelectric particles. Although elegant designs have been achieved for mechanochemically controlled RDRP based on piezocatalysis, it requires high-energy mechanical stimuli to drive the polymerization, which could inevitably induce the side reaction or impurities.[10]

Contact electrification (CE) is a well-established physical phenomenon which can be used to harvest or transform low-frequency mechanical wave into electrical or chemical signals.[11] Taking advantage of contact-electro-catalysis (CEC), many chemical reactions, such as degradation of organic dyes,[12] direct production of hydrogen peroxide,[13] reduction of metal ions,[14] and generation of flammable gases,[15] have been successfully conducted. All these processes were ascribed to the electron exchange at the interface of water and powder.[16] Under mechanical stimuli, electron exchange could occur between dielectric particles and water with repeated contact and separation cycles at the interface.[17] Electrons could flow from the water to the surface of particles, resulting in a charged interface that could efficiently catalyze chemical reactions, which usually cannot occur at normal temperature and pressure. These results indicated that contact electrification could be utilized to induce the electron transfer for the conversion of deactivators into initiating radicals for RDRP.

In this study, we proposed a facile approach for tribochemically controlled ATRP (tribo-ATRP), relying on contact-electro-catalysis between titanium oxide (TiO_2) particles and $CuBr_2$/tris(2-pyridylmethylamine (TPMA), without any high-energy input, such as ultrasound, ball milling, and ultraviolet light. Under the friction induced by stirring, the TiO_2 particles were electrified, continuously reducing $CuBr_2$/TPMA into CuBr/TPMA, thereby converting dormant alkyl halides into active growing radicals to start ATRP. In addition, the effect of friction induced by stirring on the reaction was explored by the theoretical simulation. The results indicated that elevation of frequency could reduce the energy barrier for the electron transfer from TiO_2 particles to $CuBr_2$/TPMA. Thus, the design and execution of tribo-ATRP was successfully achieved, enabling a CEC ($\approx$10 Hz) access to a variety of polymers with predetermined molecular weights, low dispersity, and high chain-end fidelity (Scheme 1).

[*] C. Wang, R. Zhao, W. Fan, Prof. Dr. L. Li, H. Feng, Z. Li, C. Yan, X. Shao, Prof. Dr. Z. Wang
Frontiers Science Center for Flexible Electronics & Xi'an Institute of Biomedical Materials and Engineering (IBME), Northwestern Polytechnical University
Xi'an 710072 (China)
E-mail: iamleili@nwpu.edu.cn
iamzhwang@nwpu.edu.cn
Prof. Dr. K. Matyjaszewski
Department of Chemistry, Carnegie Mellon University
4400 Fifth Avenue, Pittsburgh, PA 15213 (USA)
E-mail: matyjaszewski@cmu.edu

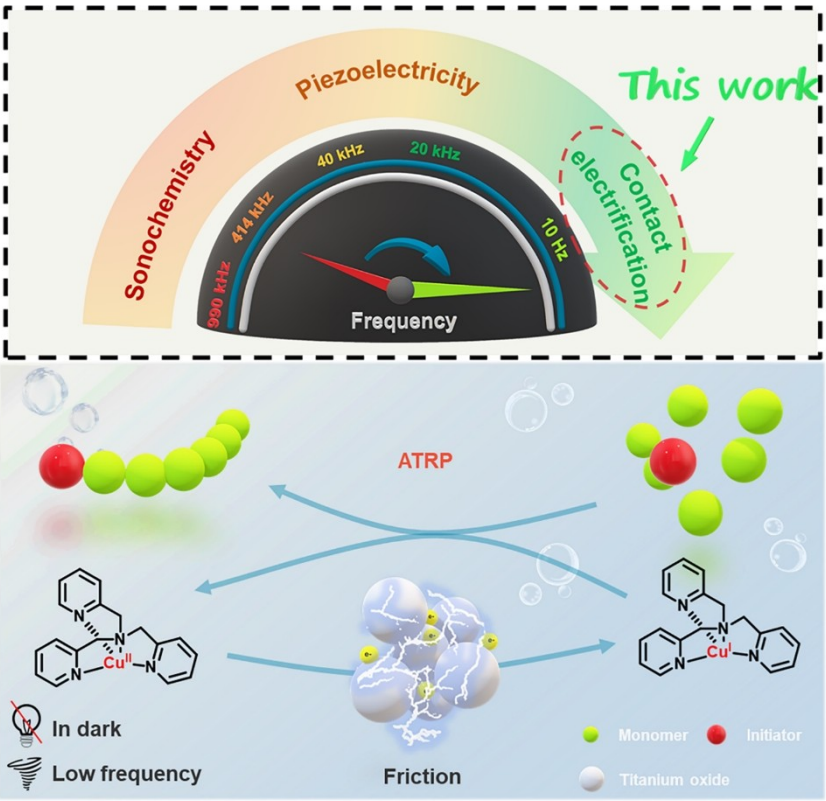

Scheme 1. Proposed mechanism of tribo-ATRP under ultralow frequency stimulation.

In ATRP, control over the polymer structure is gained through a catalytic cycle in which a low oxidation state transition-metal catalyst activates an alkyl halide to generate an alkyl radical and an oxidized form of the transition-metal complex. In most often employed systems, the activator and deactivator complexes are Cu^{I}/L and X–Cu^{II}/L, respectively. However, normal ATRP requires a high concentration of Cu^{I}/L to trigger polymerization since each radical termination event leads to the irreversible formation of the deactivator complex by the persistent radical effect. In recent years, mechanochemical approaches based on sonochemistry and piezocatalysis have been developed that allow ATRP to proceed with catalyst concentrations at or below 100 ppm.[3c,6a] The key to achieve low-ppm ATRP is the continuous reduction of the excess deactivator complex (X–Cu^{II}/L) into the activator complex (Cu^{I}/L) in the presence of mechanical force.

To confirm the pathway for the generation of the activators in this system, the UV/Vis-NIR spectra of $Cu^{II}Br_2$/TPMA were monitored before and after stirring (Figure 1a). All the reactions were conducted in the dark to eliminate the effect of light. As shown in Figure 1b, the absorption of $Cu^{II}Br_2$/TPMA remained constant without TiO_2 (Figure 1c), indicating no reduction occurred. In contrast, the intensity of the characteristic absorption band for $Cu^{II}Br_2$/TPMA in the range 550–1100 nm dramatically decreased in the presence of TiO_2 after 24 h stirring. These results suggested that TiO_2 is essential to the reduction of Br-Cu^{II}/TPMA into Cu^{I}/TPMA with the assistance of stirring.

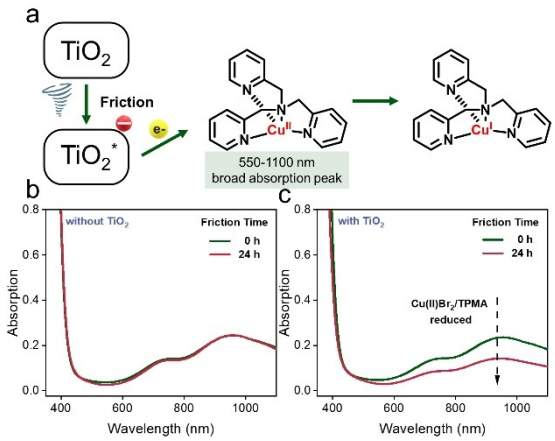

Figure 1. a) Mechanistic Scheme of the reduction of Cu^{II}. b) UV/Vis-NIR spectra without TiO_2 at different friction times. c) UV/Vis-NIR spectra with TiO_2 at different friction times. Results of UV/Vis-NIR spectra under the conditions [$CuBr_2$] = 0.75 mM, [TPMA] = 3 mM in DMSO, 2.4 wt.% TiO_2, (20–30 °C, 7 Hz).

To examine whether tribo-ATRP could proceed in the presence of TiO_2, the polymerization of methyl acrylate (MA) was initially attempted in the presence of TiO_2 using ethyl α-bromoisobutyrate (EBiB) as the initiator, $CuBr_2$/TPMA as the catalyst, and dimethyl sulfoxide (DMSO) as the solvent. Magnetic stirring was employed for generating disturbances in the reaction and increasing the probability of

contact separation. The original transparent and dilute solution became viscous after 24 h with 2.4 wt.% TiO_2, giving a poly(methyl acrylate) with number-average molecular weight (M_n) = 12 900 and dispersity ($Đ$) = 1.16 (Figure S1). In order to further investigate the mechanism of frictional electrocatalysis, we systemically investigated the factors affecting the tribo-ATRP reaction, including the loading of TiO_2, frequency of stirring, and the surface materials of stirring rods.

Initially, tribo-ATRP with varying TiO_2 loadings was performed. As shown in Figure 2b, the polymerization of MA with TiO_2 gave a linear semilogarithmic kinetic plot and excellent control over molecular weights and dispersity (Figure 2c). The rate of polymerization increased with elevating the loading of TiO_2. After 24 h stirring, the polymerization reached 45 % conversion in the presence of 0.8 wt.% TiO_2, yielding a polymer with M_n = 7 400 and $Đ$ = 1.16 (Figure S2). The conversion increased to 61 % with 1.2 wt.% TiO_2, affording a polymer with M_n = 12 300 and $Đ$ = 1.09 (Figure S3). When the TiO_2 loading increased to 2.4 wt.%, polymerization gave 80 % conversion after 24 h stir, and a polymer with M_n = 12 900 and $Đ$ = 1.16 was achieved (Figure S1). In contrast, no conversion was observed after 24 h stirring in the absence of TiO_2 (Figure S4), indicating the essential contribution of TiO_2 to the polymerization. The apparent rate constant of propagation ($k_{p,app}$) increased from 0.002 h^{-1} without TiO_2 to 0.065 h^{-1} with 2.4 wt.% TiO_2.

To investigate the effect of stirring frequency on the polymerization, a series of reactions were conducted at different stirring rate. As shown in Figure S5a, the polymerization of MA increased to 65 % conversion after 24 h at 2 Hz of stirring frequency, resulting in a well-defined polymer with M_n = 10 100 and $Đ$ = 1.14 (Figure S7). While the stirring frequency increased to 7 Hz, the conversion increased to 80 % after 24 h, and the polymer with M_n = 14 300 and $Đ$ = 1.14 was obtained (Figure S8). With further increase of stirring speed, the conversion after 24 h increased to 94 % at 13 Hz, giving a PMA with M_n = 15 800 and $Đ$ = 1.10 (Figure S9). Accordingly, the $k_{p,app}$ increased

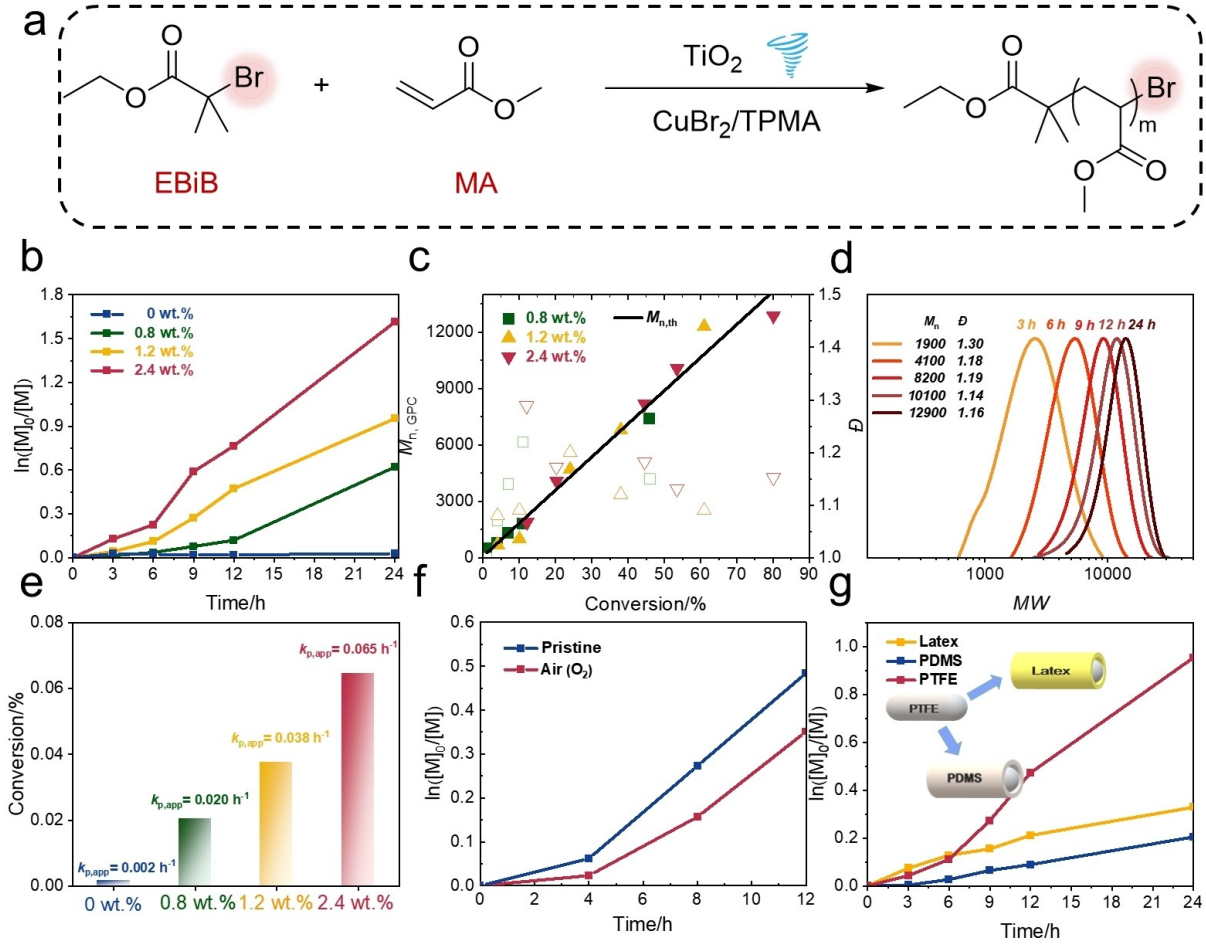

Figure 2. Results of the effect of different friction frequencies. $[MA]_0:[EBiB]_0:[CuBr_2]_0:[TPMA]_0$ = 200 : 1 : 0.03 : 0.12, in 50 % (v/v) DMSO, magnetic stirrer (20 °C ± 5 °C). b) Semi-logarithmic kinetic plot evolution of polymerization under various friction frequencies. c) The number-average molecular weight (M_n) and dispersity ($Đ$) with conversion. and d) GPC trace evolution at a friction frequency of 13 Hz. e) Results of the effect of different TiO_2 contents, under different atmospheres and with different contact surface materials. Semi-logarithmic kinetic plot evolution of polymerization with f) TiO_2 under various atmospheres (2.4 wt.% TiO_2, 12 h), and g) coated with different materials (1.2 wt.% TiO_2, 24 h).

from 0.04 h^{-1} at 2 Hz to 0.12 h^{-1} at 13 Hz. To verify that the reduction of Cu^{II} in the ATRP reaction comes from the charges generated by CEC on the TiO_2 surface rather than reductive impurities in TiO_2, tribo-ATRP with TiO_2 powders treated in different atmospheres was performed. As shown in Figure 3f, the polymerization of MA with initial TiO_2 reached 33.5 % conversion and 35.2 % conversion with TiO_2 treated in O_2 after 12 h stirring. The results showed that there was no significant difference in the effect of TiO_2 under O_2 atmosphere treatments on the polymerization rate (Figure S10–11).

To compare the effect of variation of other parameters, all subsequent experiments were performed at 7 Hz with 2.4 wt.% TiO_2 unless otherwise stated. The influence of surface materials of stir bar on the polymerization rate was compared. As manifested in Figure 2g, three magnetic stirring bars coated with different materials were used to confirm the significance of the contact materials of the magnetic bar. Among them, Bar I was a normal PTFE-sealed bar, Bar II was a bar coated with latex and Bar III was a bar coated with polydimethylsiloxane (PDMS). With the same stirring rate, higher polymerization rate was obtained by Bar I. When Bar II was used, the polymerization reduced to 28 % after 24 h, giving a PMA with M_n = 5 500 and $Đ$ = 1.17 (Figure S12). When silcone-coated bar was used, the conversion was further reduced to 18 % after

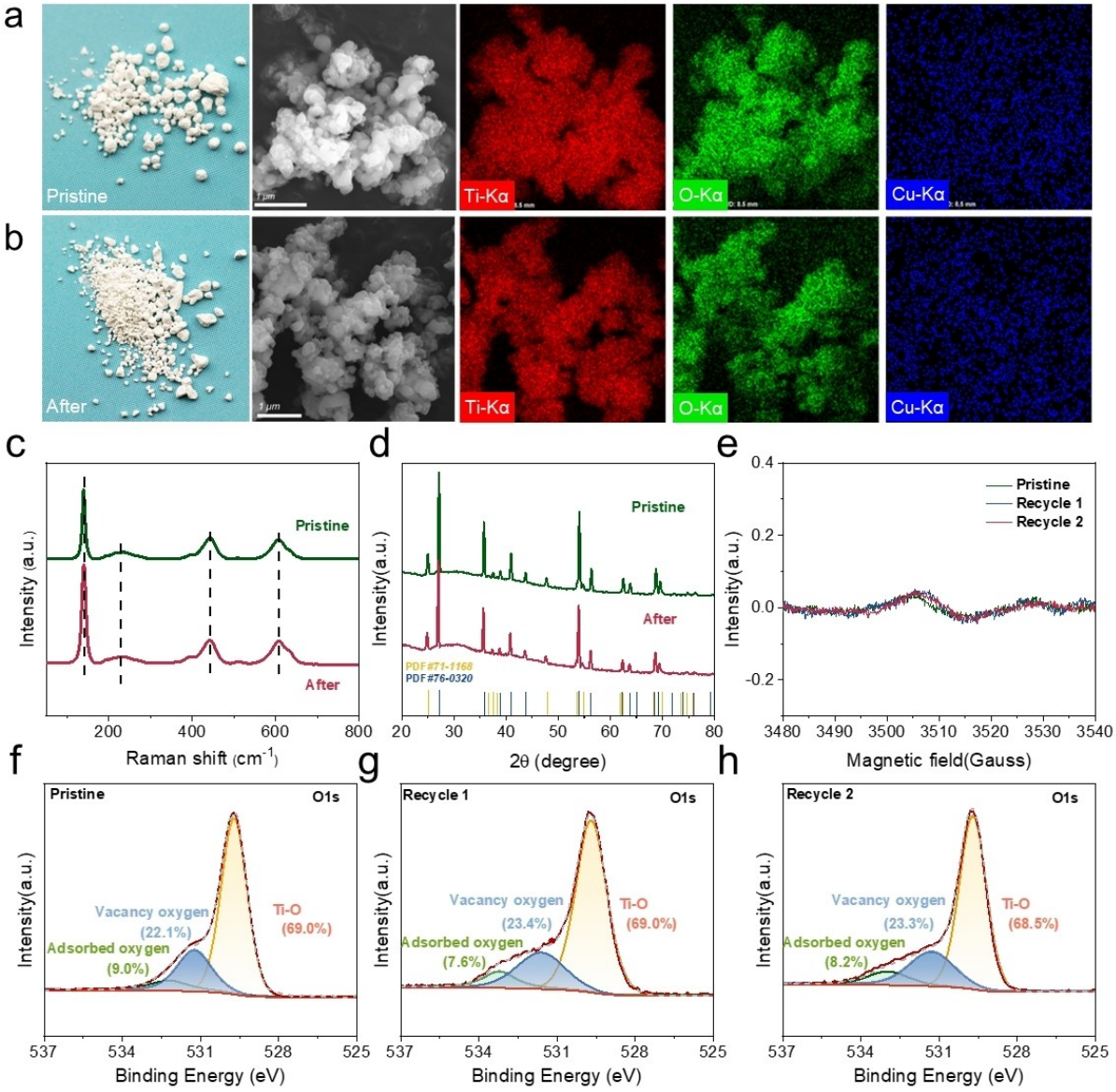

Figure 3. Characterization of TiO_2 powder before and after contact-electro-catalysis. a) Morphological characterization (SEM) and energy dispersive X-ray (EDX) analysis of the pristine TiO_2 powder before reaction, as well as b), after the reaction. c) Raman spectra of TiO_2 powder before (green) and after (red) the reaction. d) XRD patterns of TiO_2 powder before (green) and after (red) the reaction. e) EPR spectra of TiO_2 powder before (green) and after one (blue) and two (red) recycles. O1s XPS spectra of TiO_2 powder f) before and after g) one (blue) and h) two (red) recycles.

24 h at the same stirring rate, obtaining a PMA with $M_n = 2$ 000 and $Đ = 1.25$ (Figure S13). These results suggested the polymerization rate could be affected by the surface materials with varying ability to abstract electrons.

To confirm the chain-end fidelity of the polymer synthesized by this tribo-ATRP procedure, chain extension was carried out (Figure S14). The first block was conducted under identical conditions, providing a PMA-Br macroinitiator with $M_n = 14$ 600 and $Đ = 1.14$ with 88 % conversion (Figure S15). After precipitation and purification, the macroinitiator was obtained. The chain extension of PMA-Br with ethyl acrylate was conducted. After 24 h, the chain-extended polymerization was conducted, yielding of PMA-*b*-PEA-Br with $M_n = 47$ 000 and $Đ = 1.11$ (Figure S16).

Subsequently, the tribo-ATRP of MA targeting varying degrees of polymerization (*DP*) was carried out in DMSO, and the results were summarized. The concentration of monomers was maintained constant in all reactions, while the concentrations of EBiB, $CuBr_2$ and TPMA varied relative to the target DP (DP_T). As shown in in Table 1, the experimental molecular weights matched well the theoretical values. The polymerization reaction conversion was 82 % for $DP_T = 100$, giving a PMA with $M_n = 7$ 100 and $Đ = 1.09$ (entry 1, Table 1). The polymerization with $DP_T = 200$ resulted in 80 % conversion, yielding a PMA with $M_n = 14$ 300 and $Đ = 1.14$ (entry 2, Table 1). When DP_T was set at 400, the conversion reached 45 % after 24 h (entry 3, Table 1). The polymerization of MA with $DP_T = 800$ reached a conversion of 37 %, yielding a PMA with $M_n = 27$ 700 and $Đ = 1.29$ (entry 4, Table 1). This procedure could also be employed in the polymerization of other monomers, including methyl acrylate, ethyl acrylate, tert-butyl acrylate, butyl acrylate, and methyl methacrylate (entry 5–8, Table 1), yielding well-defined polymers with low dispersity and predetermined molecular weights (Figure S21–24).

To reveal the underlying mechanism of triboelectrically driven ATRP of MA, we first investigated whether the mild stirring would change the physical and chemical properties of the TiO_2 surface. Morphological characterization (SEM and TEM) and element mapping analysis of TiO_2 particles were performed before and after the reaction by scanning electron microscopy with energy dispersive X-ray analysis (SEM-EDX). From TEM images, it can be seen that TiO_2 nanoparticles present a sheet structure with a diameter of about 25 nm (Figure S25). And the specific surface area (SSA) of TiO_2 measured by Brunauer-Emmet-Teller (BET) nitrogen adsorption method was 23.74 $m^2 g^{-1}$. Figures 3a and b illustrated that neither color nor the morphology changed before/after the catalytic process. According to quantitative analysis by EDX, the surface of TiO_2 powder after reaction adsorbed a small amount of copper element (Table S1–2). Apart from morphological characterization, spectroscopic analysis techniques were also performed to deliver more in-depth information on the chemical properties of TiO_2 powder. Figure 3c present Raman spectroscopy results. In Raman spectroscopy, the skeleton vibration pattern of TiO_2 before and after the experiment was identical. X-ray diffraction (XRD) spectra of TiO_2 before/after the reaction matched well with the standards, indicating that the structure and properties of TiO_2 particles did not change after the friction process. The chemical state changes of TiO_2 particles before and after the reaction were analyzed using X-ray photoelectron spectroscopy (XPS) method. The O1s spectra of the TiO_2 powder before, after one and two recycles were listed in Figure 3 f–h, respectively. The O 1s XPS spectra of the three TiO_2 samples were deconvoluted into three peaks, corresponding to lattice oxygen (Ti–O, ≈529.7 eV), oxygen vacancies (≈531.2 eV), and chemisorbed oxygen (≈532.3 eV), respectively. It can be observed that after polymerization, the peak of Ti–O bond and oxygen vacancies did not undergo shift or change in intensity. Electron paramagnetic resonance (EPR) spectroscopy was also been used to elucidate the chemical stability of TiO_2 after tribo-ATRP. The significant peaks of three samples were detected at $g = 2.003$, and the intensities of the peaks were almost constant. This result is consistent with the aforementioned XPS result, suggesting the stability of the structure of TiO_2 particles. Zeta-potential (ξ) was further recorded. Due to the involvement of TiO_2 surface electrons in the reduction process of Cu^{II}, the value of ξ_{TiO2} increased from −11.09 mv to −8.18 mv after 1st recycle. However, after second cycle of TiO_2, the ξ of TiO_2 remained almost constant (Figure S26). This trend was similar with the evolution of catalytic efficiency for the recycled TiO_2.In the first tribo-ATRP with TiO_2, the polymerization reached a conversion of 81 % after 24 hours. When 1st recycled TiO_2 was used for tribo-ATRP, its conversion decreased to 13 % after 24 h. When the 2nd recycled TiO_2 was further used for polymer-

Table 1: Results for the polymerization of different monomers targeting various *DP*s.

Entry[a]	Monomer	DP_T	T [h]	$K_{p,\,app}$ [h^{-1}][b]	Conversion	$M_{n,\,th}$[c]	$M_{n,\,GPC}$[d]	$Đ$[d]
1	MA	100	24	0.071	82%	7,300	7,100	1.09
2	MA	200	24	0.069	80%	14,000	14,300	1.14
3	MA	400	24	0.025	45%	15,700	20,900	1.23
4	MA	800	24	0.019	37%	25,600	27,700	1.29
5	EA	200	24	0.085	87%	17,600	17,600	1.11
6	tBA	200	24	0.019	36%	9,300	12,300	1.45
7	BA	200	24	0.016	32%	8,400	10,400	1.39
8	MMA	200	24	0.014	28%	11,400	15,700	1.21

[a] Reaction conditions: $[Monomer]_0:[EBiB]_0:[Cu^{II}]_0:[TPMA]_0 = X:1:0.03:0.12$, 2.4 wt.% TiO_2, 50% v/v DMSO, magnetic stirrer (20 °C ± 5 °C, 7 Hz). [b] Conversion (*p*) was determined using ^1H NMR spectroscopy. [c] Calculated on the basis of conversion (i.e., $M_{n,th} = M_{EBiB} + [Monomer]_0/[EBiB]_0 \times conversion \times M_{monomer}$). [d] Determined using GPC in THF, based on linear PMMA as the calibration standard.

ization, the conversion dropped to 8% under standard conditions (Figure S27). As electrons on the TiO_2 surface participated in the reaction, its surface potential became more positive, giving rise to poor reductive ability for the recycled TiO_2..

CEC is proposed as the mechanism for MA polymerization in the presence of TiO_2 particles. Electrons accumulated at TiO_2* surface are captured by Cu^{II}, forming Cu^{I} to activate polymerization. To simplify the calculation, $CuBr_2$ was used for monitoring. As shown in Figure 4a, the energy barriers for realizing electron exchange processes between $CuBr_2$ and TiO_2 was assessed by Density Functional Theory (DFT). The specific calculation method is available in Method section. As shown in the Figure, under normal pressure, the wave function of LUMO energy level is on $CuBr_2$ and the HOMO energy level is on TiO_2. The energy difference between them is 0.08 eV, suggesting that the electron could hardly transfer from TiO_2 to Cu^{II} under ambient condition. While under mechanical deformation induced by stirring, the energy difference between them reached 0.97 eV, facilitating the electron transfer from TiO_2 to Cu^{II} and generating the activating complex for ATRP.

In summary, tribo-ATRP was successfully performed under moderate stirring. The results showed that surface charges accumulated on the surface of the TiO_2 under continuous stirring, continuously regenerating CuBr/TPMA (activator) from oxidized $CuBr_2$/TPMA (deactivator), and triggering ATRP. This tribo-ATRP technique allows access to the polymerization of a wide range of (meth)acrylates, yielding well-defined polymers with high end-group fidelity, predetermined molecular weights, and low dispersity. This study provides new insights for the design of green polymerizations to address the issues related to high energy consumption and ultrasonic scission.

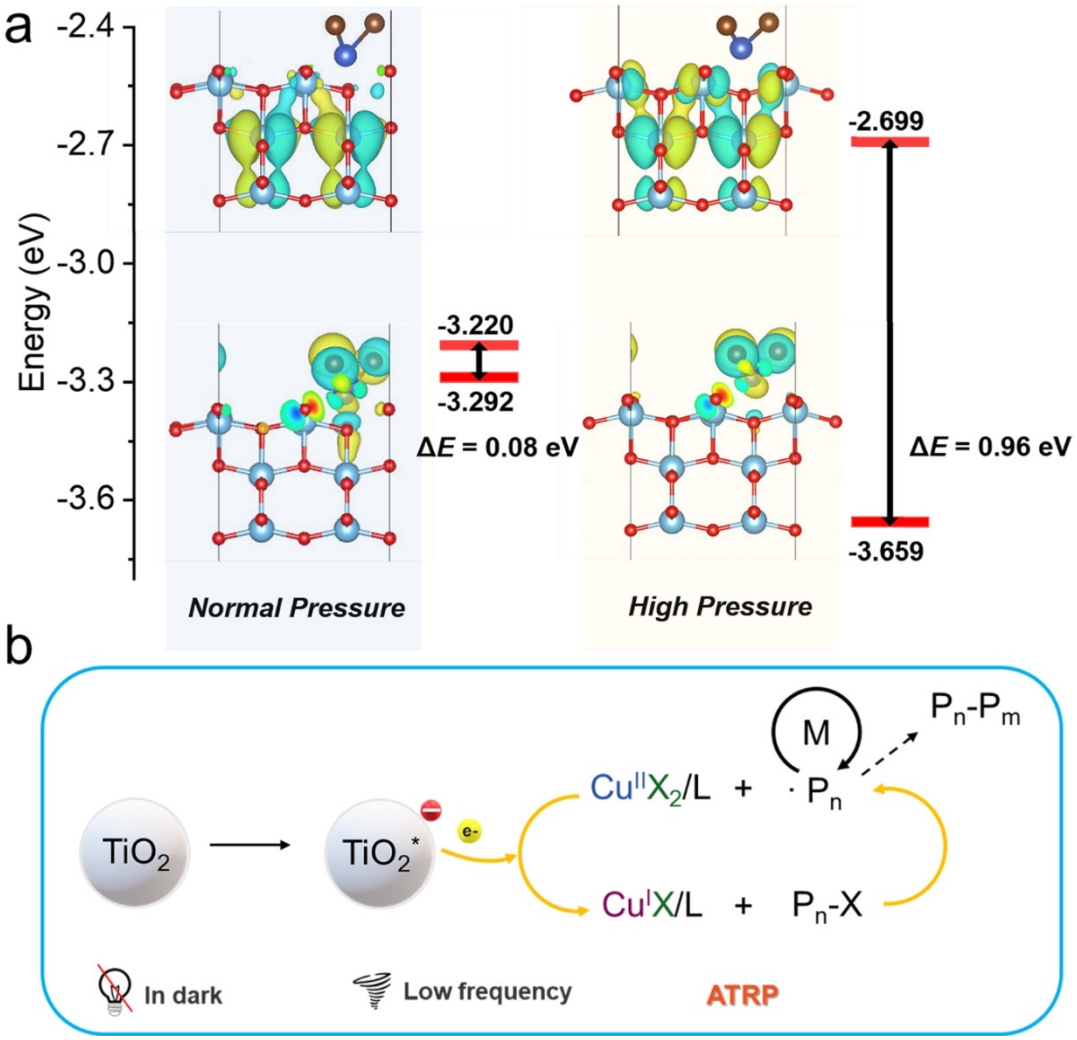

Figure 4. Mechanism of contact-electro-catalysis. a) DFT calculations of the values of LUMO and HOMO levels for TiO_2-$CuBr_2$ under various conditions as indicated by the legend. b) Proposed mechanism for the ATRP of MA by contact-electro-catalysis generated radicals.

Acknowledgements

This work was supported by the National Natural Science Foundation of China (21901207), KM acknowledges support by NSF (CHE 2000391).

Conflict of Interest

The authors declare no conflict of interest.

Data Availability Statement

The data that support the findings of this study are available in the supplementary material of this article.

Keywords: Atom Transfer Radical Polymerization · Contact Electrification · Friction · Mechanochemistry · Titanium Oxide

[1] a) K. Matyjaszewski, *Macromolecules* **2012**, *45*, 4015–4039; b) N. Corrigan, K. Jung, G. Moad, C. J. Hawker, K. Matyjaszewski, C. Boyer, *Prog. Polym. Sci.* **2020**, *111*, 101311.

[2] a) H. Mohapatra, M. Kleiman, A. P. Esser-Kahn, *Nat. Chem.* **2017**, *9*, 135–139; b) Z. Wang, J. Ayarza, A. P. Esser-Kahn, *Angew. Chem. Int. Ed.* **2019**, *58*, 12023–12026.

[3] a) Z. Wang, X. Pan, L. Li, M. Fantin, J. Yan, Z. Wang, Z. Wang, H. Xia, K. Matyjaszewski, *Macromolecules* **2017**, *50*, 7940–7948; b) Z. Wang, Z. Wang, X. Pan, L. Fu, S. Lathwal, M. Olszewski, J. Yan, A. E. Enciso, Z. Wang, H. Xia, K. Matyjaszewski, *ACS Macro Lett.* **2018**, *7*, 275–280; c) Z. Wang, F. Lorandi, M. Fantin, Z. Wang, J. Yan, Z. Wang, H. Xia, K. Matyjaszewski, *ACS Macro Lett.* **2019**, *8*, 161–165; d) C. Kütahya, C. Schmitz, V. Strehmel, Y. Yagci, B. Strehmel, *Angew. Chem. Int. Ed.* **2018**, *57*, 7898–7902; e) R. Whitfield, K. Parkatzidis, M. Rolland, N. P. Truong, A. Anastasaki, *Angew. Chem. Int. Ed.* **2019**, *58*, 13323–13328.

[4] a) T. G. McKenzie, E. Colombo, Q. Fu, M. Ashokkumar, G. G. Qiao, *Angew. Chem. Int. Ed.* **2017**, *56*, 12302–12306; b) S. Piogé, T. N. Tran, T. G. McKenzie, S. Pascual, M. Ashokkumar, L. Fontaine, G. Qiao, *Macromolecules* **2018**, *51*, 8862–8869; c) J. Collins, T. G. McKenzie, M. D. Nothling, S. Allison-Logan, M. Ashokkumar, G. G. Qiao, *Macromolecules* **2019**, *52*, 185–195; d) Q. Ma, X. Zhang, Y. Jiang, J. Lin, B. Graff, S. Hu, J. Lalevée, S. Liao, *Polym. Chem.* **2022**, *13*, 209–219; e) H. Sun, W. Choi, N. Zang, C. Battistella, M. P. Thompson, W. Cao, X. Zhou, C. Forman, N. C. Gianneschi, *Angew. Chem. Int. Ed.* **2019**, *58*, 17359–17364; f) Y. Zhao, M. Ma, X. Lin, M. Chen, *Angew. Chem. Int. Ed.* **2020**, *59*, 21470–21474.

[5] a) A. D. Jenkins, R. G. Jones, G. Moad, *Pure Appl. Chem.* **2009**, *82*, 483–491; b) A. Marathianos, E. Liarou, A. Anastasaki, R. Whitfield, M. Laurel, A. M. Wemyss, D. M. Haddleton, *Polym. Chem.* **2019**, *10*, 4402–4406; c) N. Corrigan, C. Boyer, *Trends Chem.* **2020**, *2*, 689–706.

[6] a) C. Wang, W. Fan, Z. Li, J. Xiong, W. Zhang, Z. Wang, *Polym. Chem.* **2022**, *13*, 4908–4914; b) A. R. S. Santha Kumar, A. Padmakumar, U. Kalita, S. Samanta, A. Baral, N. K. Singha, M. Ashokkumar, G. G. Qiao, *Prog. Mater. Sci.* **2023**, *136*, 101113; c) M. Nie, Q. Wang, G. Qiu, *Ultrason. Sonochem.* **2008**, *15*, 222–226; d) B. M. Teo, S. W. Prescott, G. J. Price, F. Grieser, M. Ashokkumar, *J. Phys. Chem. B* **2010**, *114*, 3178–3184; e) B. Ling, J. Lee, D. Maresca, A. Lee-Gosselin, D. Malounda, M. B. Swift, M. G. Shapiro, *ACS Nano* **2020**, *14*, 12210–12221; f) H. Mohapatra, J. Ayarza, E. C. Sanders, A. M. Scheuermann, P. J. Griffin, A. P. Esser-Kahn, *Angew. Chem. Int. Ed.* **2018**, *57*, 11208–11212; g) J. Ayarza, Z. Wang, J. Wang, C.-W. Huang, A. P. Esser-Kahn, *ACS Macro Lett.* **2020**, *9*, 1237–1248.

[7] a) M. Zhou, Y. Zhang, G. Shi, Y. He, Z. Cui, X. Zhang, P. Fu, M. Liu, X. Qiao, X. Pang, *ACS Macro Lett.* **2023**, *12*, 26–32; b) H. Y. Cho, C. W. Bielawski, *Angew. Chem. Int. Ed.* **2020**, *59*, 13929–13935; c) L. Xu, L. Xiao, P. Jia, K. Goossens, P. Liu, H. Li, C. Cheng, Y. Huang, C. W. Bielawski, J. Geng, *ACS Appl. Mater. Interfaces* **2017**, *9*, 26392–26399.

[8] K. Kubota, Y. Pang, A. Miura, H. Ito, *Science* **2019**, *366*, 1500–1504.

[9] J. Ayarza, Z. Wang, J. Wang, A. P. Esser-Kahn, *ACS Macro Lett.* **2021**, *10*, 799–804.

[10] a) X. Pan, M. Fantin, F. Yuan, K. Matyjaszewski, *Chem. Soc. Rev.* **2018**, *47*, 5457–5490; b) Y.-N. Zhou, J.-J. Li, D. Ljubic, Z.-H. Luo, S. Zhu, *Macromolecules* **2018**, *51*, 6911–6921; c) Y.-N. Zhou, J.-J. Li, Y.-Y. Wu, Z.-H. Luo, *Chem. Rev.* **2020**, *120*, 2950–3048; d) F. A. Leibfarth, K. M. Mattson, B. P. Fors, H. A. Collins, C. J. Hawker, *Angew. Chem. Int. Ed.* **2013**, *52*, 199–210; e) S. M. Zeitler, P. Chakma, M. R. Golder, *Chem. Sci.* **2022**, *13*, 4131–4138; f) M. J. Supej, B. M. Peterson, B. P. Fors, *Chem* **2020**, *6*, 1794–1803; g) Y.-N. Zhou, J.-J. Li, T.-T. Wang, Y.-Y. Wu, Z.-H. Luo, *Prog. Polym. Sci.* **2022**, *130*, 101555.

[11] a) S. Lin, X. Chen, Z. L. Wang, *Chem. Rev.* **2022**, *122*, 5209–5232; b) Y. Zhao, Y. Liu, Y. Wang, S. Li, Y. Liu, Z. L. Wang, P. Jiang, *Nano Energy* **2023**, *112*, 108464.

[12] a) Y. Zhang, T. Kang, X. Han, W. Yang, W. Gong, K. Li, Y. Guo, *Nano Energy* **2023**, *111*, 108433; b) X. Dong, Z. Wang, A. Berbille, X. Zhao, W. Tang, Z. L. Wang, *Nano Energy* **2022**, *99*, 107346; c) P. Li, J. Wu, Z. Wu, Y. Jia, J. Ma, W. Chen, L. Zhang, J. Yang, Y. Liu, *Nano Energy* **2019**, *63*, 103832; d) Z. Wang, A. Berbille, Y. Feng, S. Li, L. Zhu, W. Tang, Z. L. Wang, *Nat. Commun.* **2022**, *13*, 130; e) J. Mo, Y. Liu, Q. Fu, C. Cai, Y. Lu, W. Wu, Z. Zhao, H. Song, S. Wang, S. Nie, *Nano Energy* **2022**, *93*, 106842.

[13] a) J. Zhao, X. Zhang, J. Xu, W. Tang, Z. Lin Wang, F. Ru Fan, *Angew. Chem. Int. Ed.* **2023**, *62*, e202300604; b) B. Chen, Y. Xia, R. He, H. Sang, W. Zhang, J. Li, L. Chen, P. Wang, S. Guo, Y. Yin, L. Hu, M. Song, Y. Liang, Y. Wang, G. Jiang, R. N. Zare, *Proc. Natl. Acad. Sci. USA* **2022**, *119*, e2209056119.

[14] X. Yuan, D. Zhang, C. Liang, X. Zhang, *J. Am. Chem. Soc.* **2023**, *145*, 2800–2805.

[15] a) K.-S. Hong, H. Xu, H. Konishi, X. Li, *J. Phys. Chem. Lett.* **2010**, *1*, 997–1002; b) J. Zhang, Z. Wu, Y. Jia, J. Kan, G. Cheng, *Sensors* **2013**, *13*, 367–374.

[16] a) X. Zhang, Y. Zheng, D. Wang, Z. U. Rahman, F. Zhou, *Nano Energy* **2016**, *30*, 321–329; b) Y. Liu, Y. Zheng, T. Li, D. Wang, F. Zhou, *Nano Energy* **2019**, *61*, 454–461; c) Y. Xi, J. Wang, Y. Zi, X. Li, C. Han, X. Cao, C. Hu, Z. Wang, *Nano Energy* **2017**, *38*, 101–108.

[17] a) S. Lin, L. Xu, C. Xu, X. Chen, A. C. Wang, B. Zhang, P. Lin, Y. Yang, H. Zhao, Z. L. Wang, *Adv. Mater.* **2019**, *31*, 1808197; b) C. Xu, Y. Zi, A. C. Wang, H. Zou, Y. Dai, X. He, P. Wang, Y.-C. Wang, P. Feng, D. Li, Z. L. Wang, *Adv. Mater.* **2018**, *30*, 1706790.

Manuscript received: July 4, 2023
Accepted manuscript online: July 28, 2023
Version of record online: August 7, 2023